



Formation and structure of lithospheric shear zones with damage

W. Landuyt*, D. Bercovici

Department of Geology and Geophysics, Yale University, 210 Whitney Ave., New Haven, CT 06511, USA

ARTICLE INFO

Article history:

Received 30 October 2008

Received in revised form 4 March 2009

Accepted 6 March 2009

Keywords:

Shear localization

Damage theory

ABSTRACT

Shear localization is an integral part of tectonics on Earth. We examine the role of two different forms of microstructural weakening (voids and grain size reduction) in the formation of shear zones as a function of depth. The evolution of grain size and voids employed in this study is determined within the framework of two-phase damage theory. The shear zone model is characterized by two-dimensional simple shear, which allows for lithostatic pressure to influence the evolution of void-generating damage. We consider cases with pure void-generating damage, pure grain size reducing damage, and combined void-generating and grain size reducing damage. The introduction of lithostatic pressure alters void evolution, and specifically leads to a suppression of void-generation at depth. Grain size reducing damage produces the most significant localization. Differences in the time scale and efficacy of the two different damage mechanisms result from the mechanical constraints of viscous compaction and dilation imposed on void-generating damage. Cases with combined void-generating and grain size reducing damage lead to a more complicated interaction, with grain size reduction driving porosity to the flanks of the central shear zone. This result is proposed to be relevant for interpreting the void and grain size microstructures observed in faults on Earth.

© 2009 Elsevier B.V. All rights reserved.

1. Introduction

Concentration of deformation or shear localization is a ubiquitous feature of tectonic processes on planets. The formation of shear zones on Earth occurs on scales ranging from microns to kilometers (Regenauer-Lieb and Yuen, 2003). Plate boundaries are an example of planetary scale shear localization, hence understanding the development of shear localization is key to understanding the generation of plate tectonics (Bercovici, 2003). This long standing problem in geophysics is made considerably more difficult by the complicated interaction of tectonic forcing with poorly understood (both experimentally and theoretically) microphysical and rheological mechanisms. While the mechanisms of localization in the shallow, brittle portion of the lithosphere are reasonably well understood (Paterson, 1978), the mechanisms leading to concentration of deformation in the ductile regime remain enigmatic (e.g., Poirier, 1980).

Proposed mechanisms leading to shear localization on Earth include the coupling of viscous heating and temperature-dependent viscosity (Yuen and Schubert, 1978; Balachandar et al., 1995; Bercovici, 1996; Thatcher and England, 1998), the reduction of grain size under stress coupled with grain size sensitive viscosity (Kameyama et al., 1997; Jin et al., 1998; Braun et al., 1999;

Montesi and Hirth, 2003; Landuyt et al., 2008). Brittle and combined brittle–ductile deformation can also lead to the formation of microcracks on which deformation focuses (Ashby and Sammis, 1990; Lyakhovskiy et al., 1997; Regenauer-Lieb, 1998). Two-phase damage theory attempts to capture the physics of void-generating damage from multi-phase continuum mechanics to model ductile cracking that may lead to concentration of deformation applicable for lithospheric shear localization (Bercovici et al., 2001b; Bercovici and Ricard, 2003). Two-phase damage theory has been extended to also consider the contribution of grain size reducing damage to the development of shear localization (Bercovici and Ricard, 2005; Landuyt et al., 2008). The theory is fairly different from other elastodynamic damage (Ashby and Sammis, 1990; Lyakhovskiy et al., 1997) and grain size reduction models (Kameyama et al., 1997; Montesi and Hirth, 2003) in that the formation of void growth and grain size reduction is tracked by considering the storage of surface energy on the newly formed interface resulting from deformational work input (Bercovici et al., 2001a; Bercovici and Ricard, 2003, 2005). The assumption therefore is that some fraction of deformational work is stored by the medium through the surface energy on the generated interface (either void–rock or grain–grain), and the creation of both voids and grain size reduction results in weakening within the rock.

In this paper, we extend the study of shear localization in Earth by considering the incorporation of two-phase damage theory (Bercovici et al., 2001b; Bercovici and Ricard, 2003, 2005; Landuyt et al., 2008) into a two-dimensional simple shear model. The vari-

* Corresponding author. Tel.: +1 858 534 8771.

E-mail address: william.landuyt@yale.edu (W. Landuyt).

ation of localization mechanisms across the lithosphere is evident in experimentally inferred transitions in deformation mechanisms with depth (Kohlstedt et al., 1995). The work focuses on how the different modes of damage (i.e. void and grain size reducing damage) can lead to localization, and how these modes of localization may vary, interact or compete as a function of depth. In the context of two-phase damage rheology, the generation of voids will be suppressed at depth due to the increase in overburden (lithostatic) pressure at increasing depths. While the processes which lead to plate boundary formation should be suppressed in the mantle when transitioning from the lithosphere to asthenosphere, the two different damage mechanisms may dominate at different depths leading to variations in the concentration of deformation in the lithosphere. In this study, we focus on the effect of overburden pressure on void-generating damage and the subsequent interaction between the two forms of damage. The increase of temperature with depth in the lithosphere will tend to suppress localization due to grain size reduction (due to increasing grain growth); however we will leave this added effect for a subsequent study. By considering the interplay of void- and fineness-generating damage in a simplified model we are able to understand the physics of shear localization which may arise within the lithosphere.

2. Two-phase damage theory: review and current formulation

The two-phase damage equations originate from a series of papers (Bercovici et al., 2001a,b; Ricard et al., 2001), with subsequent papers refining various aspects of the theory (Ricard and Bercovici, 2003; Bercovici and Ricard, 2003, 2005). The equations are in the geologically applicable “void limit” as discussed in (Ricard and Bercovici, 2003), whereby the void phase has zero density, pressure and viscosity.

2.1. Mass

The equation for mass conservation is

$$\frac{D\phi}{Dt} = \frac{\partial\phi}{\partial t} + \mathbf{v} \cdot \nabla\phi = (1 - \phi)\nabla \cdot \mathbf{v} \quad (1)$$

where \mathbf{v} is the matrix (or rock phase) velocity and ϕ is the porosity. In the void limit the velocity of the void phase is the same as the matrix velocity.

2.2. Momentum

The momentum equations are

$$0 = \nabla[-(1 - \phi)P + \sigma\alpha] + \nabla \cdot [(1 - \phi)\underline{\tau}] - (1 - \phi)\rho g \hat{\mathbf{z}} \quad (2)$$

where P is the matrix pressure, σ is the surface tension, α is the interfacial area density, $\underline{\tau}$ is the deviatoric matrix stress, and ρ is the density of the matrix phase. A novel component of this work is the effect of overburden pressure on void-generating damage, and this effect arises from the inclusion of the term proportional to ρg in (2). The deviatoric stress is given by

$$\underline{\tau} = \mu \left[\nabla\mathbf{v} + [\nabla\mathbf{v}]^t - \frac{2}{3}(\nabla \cdot \mathbf{v})\mathbf{I} \right] \quad (3)$$

where μ is the viscosity, and \mathbf{I} is the identity matrix. The interfacial area density is a function of porosity (ϕ) and inverse grain size (A), and its functional form reflects assumptions about the underlying two-phase microstructure. In previous studies (Bercovici et al., 2001b; Bercovici and Ricard, 2003; Ricard and Bercovici, 2003; Landuyt et al., 2008) the functional form of α employed was

$$\alpha(\phi, A) = A\phi^a(1 - \phi)^b, \quad (4)$$

where at the end member values of porosity ($\phi = 0, 1$) α goes to zero. The microstructural model described by Eq. (4) therefore states that there cannot be interfacial area within a single phase (e.g. grain boundaries). Here, we consider microstructural models that allow for grain–grain interfaces to contribute to the interfacial area density. We therefore employ the functional form

$$\alpha(\phi, A) = A\eta(\phi) = A(\phi_o + \phi)^a(1 - \phi)^b, \quad (5)$$

where ϕ_o is a constant, a and b are between 0 and 1, and α goes to zero at $\phi = 1$ and remains non-zero at $\phi = 0$, thereby allowing for grain–grain boundaries to contribute to the interfacial area density. This formulation for the variations in interfacial area density as a function of porosity is similar to previous considerations with matrix and melt distributions (Hier-Majumder et al., 2006). We will choose $\phi_o = 0.25$ and $a = b = 0.5$ for all simulations in this study. Following the previous formulations of the matrix rheology we assume the lithospheric viscosity is given by

$$\mu = \mu_o \left(\frac{A_o}{A} \right)^m \quad (6)$$

where A_o is a reference value for fineness and μ_o is a reference viscosity characteristic of the zeroth order behavior of the lithosphere. The viscosity exponent m is a dimensionless positive constant; assuming operation of a grain size sensitive deformation mechanism (e.g. diffusion creep) suggests that $m = 2 - 3$. While the lithosphere is generally believed to obey dislocation creep (and hence a grain size insensitive rheology), we assume the medium has a grain size sensitive viscosity, which can be accomplished by having a statistical average of creep mechanisms over grain size distribution (e.g. large grains undergo dislocation creep and small grains undergo diffusion creep) (Ricard and Bercovici, 2009). Field and experimental work have also shown that lithospheric rocks with a given grain size distribution can partially deform by dislocation creep but have the rheology controlled by the weaker diffusion creep (and hence grain size sensitive) portion (Jin et al., 1998). Given the momentum Eq. (2) we find that the effective matrix viscosity is given by

$$\mu_{\text{eff}} = (1 - \phi)\mu = \mu_o(1 - \phi) \left(\frac{A_o}{A} \right)^m \quad (7)$$

where the $(1 - \phi)$ factor in the viscosity arises from the deviatoric stress term in (2).

2.3. Energy

The energy equation is separated into two coupled equations which govern the evolution of thermal energy and the rate of work done on the interface by pressure, surface tension and deformational work (Bercovici and Ricard, 2005). The evolution of thermal energy is (with our assumptions above)

$$\begin{aligned} (1 - \phi)\rho c \frac{DT}{Dt} - T \frac{D}{Dt} \left(\alpha \frac{d\sigma}{dT} \right) - T\alpha \frac{d\sigma}{dT} \nabla \cdot \mathbf{v} \\ = Q - \nabla \cdot \mathbf{q} + \mathcal{B} \left(\frac{D\phi}{Dt} \right)^2 + \sigma\eta k_A A^p + (1 - f)\Psi \end{aligned} \quad (8)$$

where T is the temperature, c is the matrix heat capacity, $(-d\sigma/dT)$ is the interfacial entropy per unit area, \mathbf{q} is an energy flux vector (e.g. heat diffusion), and Q is an intrinsic heat source. The quantity \mathcal{B} is positive, has units of viscosity, and is related to the bulk viscosity term in the two-phase theory of McKenzie (1984); the term proportional to \mathcal{B} represents irreversible work done during isotropic compression or dilation. Following previous formulations for \mathcal{B} in the evacuated void limit we arrive at

$$\mathcal{B} = \frac{K\mu_o}{\phi(1 - \phi)} \quad (9)$$

where K is a dimensionless factor accounting for pore or grain geometry and is typically $\mathcal{O}(1)$ (Bercovici et al., 2001a; Bercovici and Ricard, 2005). The quantity k_A represents the rate of grain growth (Karato, 1989); the term proportional to k_A represents the contribution of irreversible loss of interfacial area (via grain growth) to the evolution of thermal energy. The viscous deformational work is given by

$$\Psi = (1 - \phi) \nabla \mathbf{v} : \underline{\underline{\tau}}, \quad (10)$$

a fraction $1 - f$ of which is partitioned into dissipative heating. The evolution of energy associated with the interface is

$$\sigma \frac{D\alpha}{Dt} = -P \frac{D\phi}{Dt} - \mathcal{B} \left(\frac{D\phi}{Dt} \right)^2 - \sigma \eta k_A A^p + f \Psi. \quad (11)$$

Since changes in α can be manifested as either changes in porosity or changes in inverse grain/void size we can decompose (11) into one damage evolution equation for porosity and one for grain size (Bercovici and Ricard, 2005). Employing the model for interfacial area density in (5) we associate derivatives of ϕ with the terms associated with volume change and derivatives of A with the terms associated with grain size change. The damage equation for porosity is

$$\sigma A \frac{d\eta}{d\phi} \left(\frac{D\phi}{Dt} \right) = -P \left(\frac{D\phi}{Dt} \right) - \mathcal{B} \left(\frac{D\phi}{Dt} \right)^2 + f_\phi \Psi, \quad (12)$$

and the evolution equation for fineness is

$$\frac{DA}{Dt} = \frac{f_A}{\sigma \eta} \Psi - k_A A^p, \quad (13)$$

where $f = f_\phi + f_A$ must be less than or equal to one. We assume that the term proportional to k_A is directly related to changes in A (i.e. grain/void size) and not the void volume fraction, hence the healing term is only in (13). We will consider cases where each damage mechanism operates by itself as well as in tandem with the other damage mechanism. The partitioning fraction of damage in the void-generating case is given by

$$f_\phi = f^* \frac{(D\phi/Dt)^2}{\gamma + (D\phi/Dt)^2} \quad (14)$$

where f^* is the maximum permissible f_ϕ , γ controls the variability of f_ϕ , and f_ϕ is assumed to depend on an even power of $D\phi/Dt$ since it must be positive definite. As previously discussed in Bercovici et al. (2001b) and Bercovici and Ricard (2003), the above equation for f_ϕ precludes singular solutions of the porosity damage equation (12) in areas of zero void growth (i.e. $D\phi/Dt = 0$).

3. Shear zone model

3.1. Formulation

We examine two-dimensional simple shear calculations to understand the formation and evolution of depth-dependent structure in a shear zone (see Fig. 1). The domain is infinitely long in the x -direction, $2L$ wide in the y -direction ($-L < y < +L$), and a height of D in the vertical direction ($-D < z < 0$). All of the boundaries are impermeable ($v_y = 0$ at $y = \pm L$ and $v_z = 0$ at $z = -D, 0$). The boundaries at $z = -D, 0$ are free-slip (i.e. $\partial v_x / \partial z = \partial v_y / \partial z = 0$). The boundaries at $y = \pm L$ are free-slip for vertical motion (i.e. $\partial v_z / \partial y = 0$) but driven by no-slip, constant velocity conditions in the horizontal direction ($v_x(y = \pm L) = \pm U_{max}$); the combination of boundary conditions on the side walls ($y = \pm L$) allows vertical displacement/deformation on the horizontally moving boundary. All of the dependent variables depend only on y, z and t . To non-dimensionalize the above equations we choose a time scale given by $4\mu_o/3\sigma A_o$ (where A_o is the inverse length scale for inverse grain

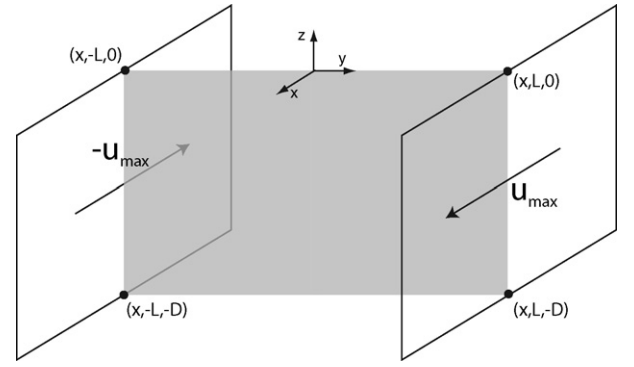


Fig. 1. The shear zone model employed in this study.

size), spatial length scale D , and pressure by σA_o . We define $(u, v, w) = (4\mu_o/3\sigma A_o D)(v_x, v_y, v_z)$ and $\mu_e = \mu_{eff}/\mu_o$. The non-dimensional continuity Eq. (1) becomes

$$\frac{\partial \phi}{\partial t} = \frac{\partial}{\partial y} ((1 - \phi)v) + \frac{\partial}{\partial z} ((1 - \phi)w). \quad (15)$$

The non-dimensional forms of the x -, y -, and z -components of momentum with (12) substituted into the pressure term become

$$0 = \frac{\partial}{\partial y} \left(\mu_e \frac{\partial u}{\partial y} \right) + \frac{\partial}{\partial z} \left(\mu_e \frac{\partial u}{\partial z} \right), \quad (16)$$

$$\begin{aligned} & - \left(\frac{\partial}{\partial y} (A\lambda) + \frac{\partial F\Psi'}{\partial y} \right) \\ & = \left[\frac{\partial}{\partial y} \left(\zeta(\phi, A) \frac{\partial v}{\partial y} \right) + \frac{\partial}{\partial z} \left(\frac{3\mu_e}{4} \frac{\partial v}{\partial z} \right) \right] + \frac{\partial \xi(\phi, A)}{\partial y} \frac{\partial w}{\partial z} \\ & \quad + \frac{3}{4} \frac{\partial \mu_e}{\partial z} \frac{\partial w}{\partial y} + \left(\frac{3\mu_e}{4} + \xi(\phi, A) \right) \frac{\partial^2 w}{\partial y \partial z}, \end{aligned} \quad (17)$$

$$\begin{aligned} & B(1 - \phi) - \left(\frac{\partial}{\partial z} (A\lambda) + \frac{\partial F\Psi'}{\partial z} \right) \\ & = \left[\frac{\partial}{\partial z} \left(\zeta(\phi, A) \frac{\partial w}{\partial z} \right) + \frac{\partial}{\partial y} \left(\frac{3\mu_e}{4} \frac{\partial w}{\partial y} \right) \right] + \frac{\partial \xi(\phi, A)}{\partial z} \frac{\partial v}{\partial y} \\ & \quad + \frac{3}{4} \frac{\partial \mu_e}{\partial y} \frac{\partial v}{\partial z} + \left(\frac{3\mu_e}{4} + \xi(\phi, A) \right) \frac{\partial^2 v}{\partial y \partial z}, \end{aligned} \quad (18)$$

where

$$\lambda = \eta(\phi) + (1 - \phi) \frac{d\eta}{d\phi}, \quad (19)$$

$$\zeta(\phi, A) = (1 - \phi) \left(\frac{3K}{4\phi} + \frac{1}{A^m} \right),$$

$$\xi(\phi, A) = (1 - \phi) \left(\frac{3K}{4\phi} - \frac{1}{2A^m} \right),$$

$$F = \frac{3f^*}{4} \frac{(1 - \phi)^2 (\nabla \cdot \mathbf{v})}{\gamma + (1 - \phi)^2 (\nabla \cdot \mathbf{v})^2},$$

$$\Psi' = (1 - \phi) \left(\nabla \mathbf{v} : (\nabla \mathbf{v} + [\nabla \mathbf{v}]^t - \frac{2}{3} (\nabla \cdot \mathbf{v}) \mathbf{I}) \right).$$

The non-dimensional parameter

$$B = \frac{\rho g D}{\sigma A_o} \quad (20)$$

is the Bond number and represents the hydrostatic pressure variations relative to interfacial surface tension forces. In the context of our shear zone model the Bond number dictates the depth to which voids (or mode-I cracks) will exist. The non-dimensional equation for porosity is identical to (15), and the non-dimensional fineness evolution equation is

$$\frac{DA}{Dt} = \frac{f_A}{\eta(\phi)} \mu_e \Psi' - \hat{k}_A A^p, \quad (21)$$

where $\hat{k}_A = 4\mu_o A_o k_A / (3\sigma)$.

3.2. Linear stability analysis

The linear stability analysis for the one-dimensional simple shear void-generating damage problem has been done in Bercovici et al. (2001b) and Bercovici and Ricard (2003). We examine the initiation of fineness controlled shear localization from an infinitesimal perturbation. We will neglect the depth dependence of the system equations and focus on simple 1D equations to simplify the linear stability analysis, therefore the vertical velocity w and all derivatives with respect to z are zero. We will also neglect void-generating damage for the sake of convenience. We assume the medium to have a basic state (u_o , A_o , and ϕ_o), and we write the variables as $u = u_o + \epsilon u_1$, $v = \epsilon v_1$, $A = A_o + \epsilon A_1$, and $\phi = \phi_o + \epsilon \phi_1$. There are two equations of zeroth order in ϵ (\hat{x} momentum equation and fineness evolution),

$$0 = \frac{\partial}{\partial y} \left(\frac{1 - \phi_o}{A_o^m} \frac{\partial u_o}{\partial y} \right) \Rightarrow \frac{1 - \phi_o}{A_o^m} \frac{\partial u_o}{\partial y} = \Omega = \text{const} \quad (22)$$

$$A_o^{p-m} = \frac{3}{4} \frac{f_A \Omega^2}{\hat{k}_A \eta(\phi_o)} \frac{1}{1 - \phi_o}. \quad (23)$$

The zeroth order fineness equation (23) suggests that the magnitude of fineness reached in simple shear is a function of the ratio of damage (f_A) to healing (\hat{k}_A) as previously mentioned by Landuyt et al. (2008). We could alternatively write the dependence of fineness on strain-rate (u_o/δ , where δ is the shear zone width) instead of stress (Ω) and arrive at $A_o^{p+m} \sim f_A (u_o/\delta)^2 / \hat{k}_A$. To first order in ϵ the system of equations become,

$$\frac{\partial \phi_1}{\partial t} = (1 - \phi_o) \frac{\partial v_1}{\partial y} \quad (24)$$

$$0 = \frac{1 - \phi_o}{A_o^m} \frac{\partial^2 u_1}{\partial y^2} - m \frac{\Omega}{A_o} \frac{\partial A_1}{\partial y} - \frac{\Omega}{1 - \phi_o} \frac{\partial \phi_1}{\partial y} \quad (25)$$

$$0 = \lambda(\phi_o) \frac{\partial A_1}{\partial y} + \left(A_o \frac{d\lambda(\phi_o)}{d\phi_o} \right) \frac{\partial \phi_1}{\partial y} + (1 - \phi_o) \left[\frac{3K}{4\phi_o} + A_o^{-m} \right] \frac{\partial^2 v_1}{\partial y^2} \quad (26)$$

$$\begin{aligned} \frac{\partial A_1}{\partial t} = & \frac{f_A}{\eta(\phi_o)} \left[\frac{3}{2} \Omega \frac{\partial u_1}{\partial y} - \frac{3m\Omega^2}{4} \left(\frac{A_o^m}{1 - \phi_o} \right) \frac{A_1}{A_o} \right. \\ & \left. - \frac{3\Omega^2}{4} \left(\frac{A_o^m}{1 - \phi_o} \right) \frac{\phi_1}{1 - \phi_o} \right] - \hat{k}_A p A_o^{p-1} A_1, \end{aligned} \quad (27)$$

where we have used (22) to simplify the equations. Assuming that u_1 , v_1 , ϕ_1 , and A_1 go as e^{iky+st} , we arrive at the following equation for the growth rate (s)

$$\begin{aligned} s = & -\frac{1}{2} \left((p-m) \hat{k}_A A_o^{p-1} + A_o \frac{d\lambda(\phi_o)}{d\phi_o} \frac{1}{((3K/4\phi_o) + A_o^{-m})} \right) \\ & \pm \frac{1}{2} \left((p-m)^2 \hat{k}_A^2 A_o^{2(p-1)} + A_o^2 \left(\frac{d\lambda(\phi_o)}{d\phi_o} \right)^2 \frac{1}{((3K/4\phi_o) + A_o^{-m})^2} \right. \\ & \left. - 2 \frac{\hat{k}_A A_o^p}{1 - \phi_o} \frac{1}{((3K/4\phi_o) + A_o^{-m})} \{ (p-m)(1-\phi_o) \frac{d\lambda(\phi_o)}{d\phi_o} + 2\lambda(\phi_o) \} \right)^{\frac{1}{2}}. \end{aligned} \quad (28)$$

The growth rate has two roots, and for the negative square root the growth rate is always less than zero. For the positive square root, the sign of s is positive and its magnitude grows with increasing f_A (damage) and Ω (stress). Linear stability analysis therefore predicts that fineness-generating damage will allow for some solutions to grow unstably (and potentially lead to shear localization), and the growth rate of this perturbation increases with increasing damage. The entire growth rate is real; this is noteworthy because if it were complex it would indicate that perturbations in the field variables (A , ϕ) are out of phase. We see later in the finite amplitude case (Section 4.3) that these variables are significantly out of phase.

3.3. Amplitude analysis

We now examine an approximate solution for the growth of a fineness anomaly when we consider the 1D version of our simple shear model discussed in the linear stability analysis. We will not repeat the analysis for the growth of a porosity anomaly since this was already done in Bercovici et al. (2001b), and as is shown in the numerical results of this study the fully non-linear analysis yields void and fineness fields that have complicated spatial interactions which suggest an amplitude analysis is of little utility. We further assume that porosity is constant and focus on the competition between damage input and healing for fineness (neglecting advection of fineness). The fineness evolution equation becomes

$$\frac{dA}{dt} = \mathcal{D} A^m - \hat{k}_A A^p, \quad (29)$$

where $\mathcal{D} = c f_A \Omega^2$, c is a constant of order one, and Ω^2 goes as $(1/A^{2m})(U_{max}/l)^2$, where l is the length scale over which shear localization occurs. Separating out the fineness and time dependence of (29) and integrating we arrive at

$$\int_{A_i}^A \frac{dA'}{A'^m (\mathcal{D} - \hat{k}_A A'^{p-m})} = t, \quad (30)$$

where A_i is the initial value of fineness at $t = 0$. For the choices of p and m we consider here ($p = 3$, $m = 2$) (30) results in the following implicit solution,

$$\frac{\hat{k}_A}{\mathcal{D}} \log \left(A \frac{(\mathcal{D}/\hat{k}_A) - 1}{(\mathcal{D}/\hat{k}_A) - A} \right) + \frac{A - 1}{A} = \mathcal{D} t, \quad (31)$$

where we have assumed that $A_i = 1$ at $t = 0$. Solutions reach a steady state value $A = (\mathcal{D}/\hat{k}_A)^{1/(p-m)}$, which is predicted by the linear stability analysis as well (see (23)). Since the damage constant \mathcal{D} multiplies time, the magnitude of damage will have a strong control on the temporal evolution of fineness. Inspection of (31) implies that the magnitude of damage fraction controls the time scale for shear zone formation (when grain size controls the rheology), and the ratio of damage to healing will control the final degree or amount of localization attained (see Fig. 2). This result makes physical sense since grain growth would likely be smaller than damage input when deformation commences, since grain sizes are initially large and uniform. When deformational work decreases grain size substantially, grain growth then becomes comparable to damage

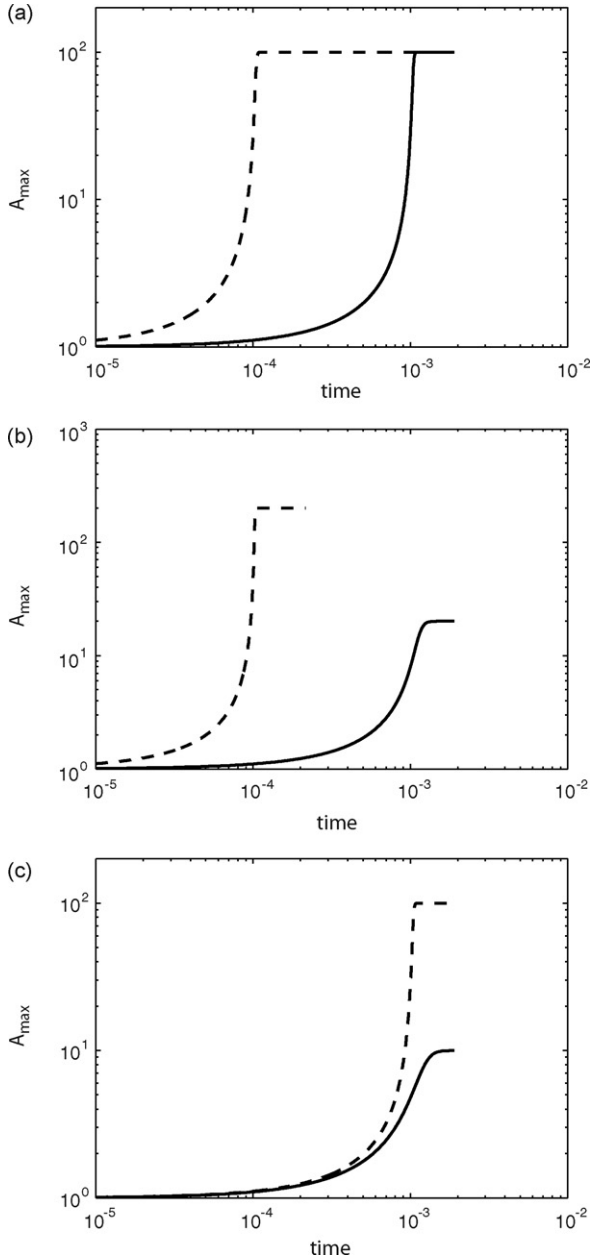


Fig. 2. Results from the amplitude analysis for the evolution of fineness. (a) The evolution of fineness over time with constant ratio of damage (\mathcal{D}) to healing (\hat{k}_A), but with different magnitudes of \mathcal{D} and \hat{k}_A ($\mathcal{D} = 10^3$ and $\hat{k}_A = 10^1$ (solid), and $\mathcal{D} = 10^4$ and $\hat{k}_A = 10^2$ (dash)). (b) The evolution of fineness over time with constant healing ($\hat{k}_A = 50$) but increasing values of damage ($\mathcal{D} = 10^3$ (solid) and $\mathcal{D} = 10^4$ (dash)). (c) The evolution of fineness over time with constant damage ($\mathcal{D} = 10^3$) but increasing values of healing ($\hat{k}_A = 10^1$ (dash) and $\hat{k}_A = 10^2$ (solid)).

input and the balance between the two leads to a stabilization of fineness and hence localization ceases.

4. Numerical results

The equations for u , v , and w are numerically solved via a finite volume, multigrid method. Given the fineness and porosity field, the horizontal velocity u is readily calculated. Since v and w are coupled, their solutions are obtained by iterating on (17) and (18) until convergence (defined to be when the L_∞ norm of successive iterations for v and w reaches 10^{-3} or less). For simulations with non-zero f_ϕ , we treat the term proportional to $F\Psi'$ in (17) and (18) as a forcing function to a Poisson's equation with

non-constant coefficients. Initially simulations required on average approximately 10–20 iterations for convergence (though this value increases (decreases) with increasing (decreasing) f_A and f^*), though as they approached steady state one to two iterations was sufficient for convergence. We benchmark the code by comparing numerical solutions to analytical solutions obtained when both A and ϕ are constant throughout the domain. Given the solutions for v and w , A and ϕ are then updated using (21) and (15), respectively. Numerical simulations are run with a resolution of either 129 or 257 points in the horizontal direction and 65 or 129 points in the vertical direction to ensure sufficient resolution of shear localizing features.

4.1. Fineness-generating damage

We now explore the full non-linear solutions with fineness-generating damage by itself before we attempt to understand how the two damage mechanisms interact and lead to localization simultaneously. The simulations were initiated with a fineness anomaly given by

$$A(t=0) = A_i + A_p \exp(-y^2/\delta_A), \quad (32)$$

where $A_i = 1.0$, $A_p = 0.25$, $\delta_A = 1$, and the porosity field is a constant value of 0.05 throughout. For the sake of clarity we do not explore all of parameter space and focus on how shear zone evolution is controlled by a few parameters; specifically we vary the shearing rate (U_{\max}) and the values of damage (f_A) and healing rate (\hat{k}_A). We will assume that the exponent p in (13) associated with surface tension driven grain growth is three, and the exponent characterizing the sensitivity of viscosity to grain size (m) is three as well. While we assumed that $m = 2$ in the amplitude analysis, we have run full numerical simulations with both $m = 2$ and 3 and there is no significant difference between the two cases (though $m = 3$ does lead to more localization of shear). Since we are neglecting the effect of variations in temperature with depth in this study, the fineness field is only weakly dependent on depth through porosity.

The amplitude analysis for fineness-generating damage suggests that the time scale for shear zone formation will be a function of damage fraction (f_A), and both the amplitude analysis and linear stability analysis suggest the amount of grain size reduction and hence localization will be a function of the relative amounts of damage to healing. While maintaining a constant ratio of f_A/\hat{k}_A but increasing the absolute magnitudes of f_A and \hat{k}_A , the time for shear zone formation decreases (see Fig. 3a). While the absolute magnitude of f_A and \hat{k}_A affect the time evolution, the concentration of deformation (Fig. 3b) and fineness field (Fig. 3c) remain unchanged. The result that shear localization does not change while the damage to healing ratio is held constant is consistent with the amplitude analysis and the linear stability analysis since the zeroth order term for fineness goes as the ratio of f_A to \hat{k}_A (see (27)).

The effect of increasing the shearing rate (U_{\max}) results in a decrease in shear zone formation time (see Fig. 4a). Similar to the previous result of increasing f_A and \hat{k}_A in step, increasing U_{\max} by an order of magnitude causes the timescale for shear zone evolution to decrease by approximately an order of magnitude. Changing U_{\max} causes a change in the strain-rate, and hence influences the fineness since $A \sim U_{\max}^{2/(p+m)}$ (see Section 3.2), which produces a similar result as increasing the damage fraction f_A . This increase in damage input results in a greater concentration of deformation (Fig. 4b) and significantly more grain size reduction (Fig. 4c). Conversely, by increasing the healing rate, shear localization is mitigated (Fig. 5b) and grain size variations become less pronounced (Fig. 5c). The time for shear zone formation is essentially insensitive to changes in healing rate, in accord with the amplitude analysis. These results reaffirm the previous suggestion that damage input controls the

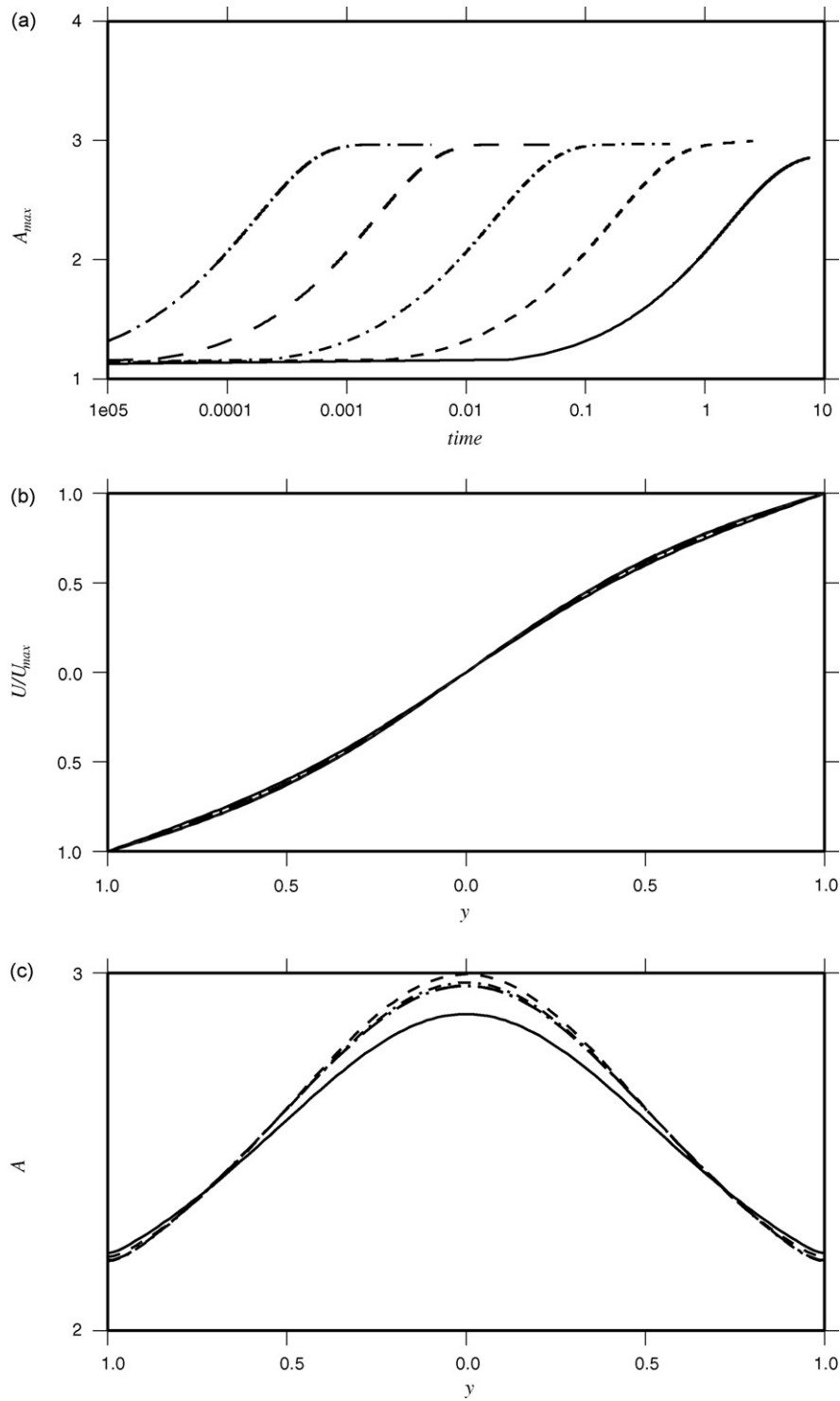


Fig. 3. (a) The maximum value of fineness versus time for constant damage to healing ratio, but with different values of damage and healing. The value of f_A/\hat{k}_A is 10^{-3} with $f_A = 10^{-1}$ (long dash-dot), 10^{-2} (long dash), 10^{-3} (short dash-dot), 10^{-4} (short dash), and 10^{-5} (solid). (b) The velocity into the shear zone, u , as a function of the differing damage and healing values at a depth of $z = -0.5$. (c) The fineness across the shear zone at a depth of $z = -0.5$.

time scale for shear zone formation, and the competition between damage and healing determines the overall amount of localization achieved in the shear zone.

4.2. Void-generating damage

A novel component of this study is the consideration of depth-dependent processes on shear zone formation with a two-phase damage rheology, hence we now consider the evolution of porosity

under the influence of both gravity and void-generating damage. Numerical simulations are run with a resolution of either 129 or 257 points in the horizontal direction and 65 or 129 points in the vertical direction. The simulations were initiated with a porosity anomaly given by

$$\phi(t = 0) = \phi_i + \phi_p \exp\left(\frac{-y^2}{\delta_p}\right), \quad (33)$$

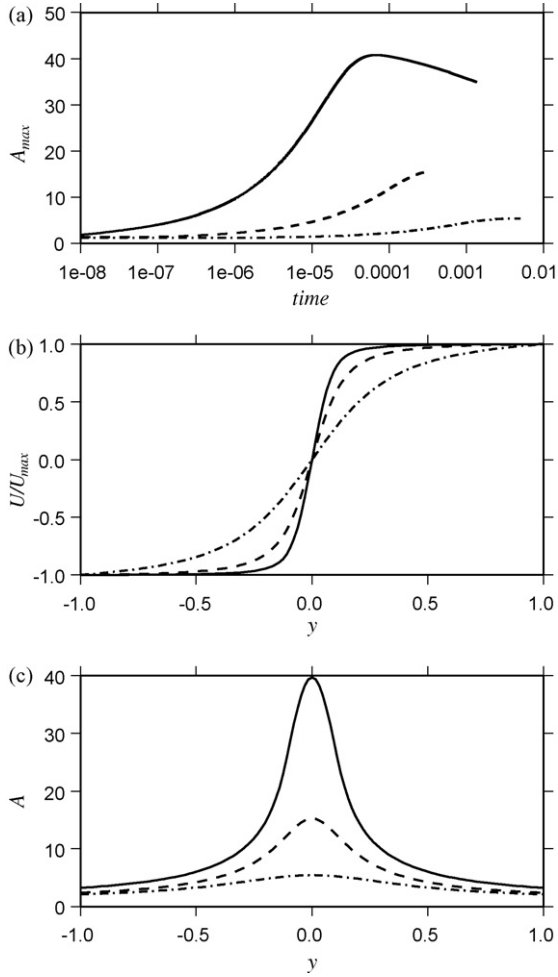


Fig. 4. (a) The maximum and minimum values of fitness versus time for constant damage to healing ratio, but with different values of shearing rate (U_{max}). The value of f_A/\hat{k}_A is 10^{-2} with $f_A = 10^{-1}$ and $\hat{k}_A = 10^1$, and the three different values of U_{max} are 5×10^2 (dash-dot), 5×10^3 , (dash), and 5×10^4 (solid). (b) The velocity into the shear zone, u , as a function of the horizontal coordinate y at a depth of $z = -0.5$. (c) The fitness across the shear zone at a depth of $z = -0.5$.

where $\phi_i = 0.05$, $\phi_p = 0.01$, $\delta_p = 1$, and the fitness field is a constant value of 1.0 throughout. We will later adjust ϕ_i , ϕ_p , and δ_p when we consider combined void- and fitness-generating damage.

Since overburden pressure will act to close voids at depth, localization due to void-generating damage should be suppressed at depth. As shown in Ricard et al. (2001), Bercovici et al. (2001b) and Bercovici and Ricard (2003), there is phase separation even without shear and/or damage. In the absence of both gravity and damage the porosity profiles of self-separation (i.e. no damage) reproduce the smooth, well-rounded porosity profiles (Fig. 6(a1)) seen in previous one-dimensional studies (Bercovici and Ricard, 2003). The effect of damage ($f^* \neq 0$) in the absence of gravity reproduces both the weak and strong localization (Fig. 6(b1) is an example of strong porosity localization) regimes of one-dimensional studies (Bercovici and Ricard, 2003).

The presence of gravity, the strength of which is determined by the Bond number, breaks up the vertical symmetry of porosity evolution. Without damage, the evolution of porosity involves a competition between surface tension and gravitational forces. With increasing Bond number the porosity field begins to spread out along the top surface of the domain due to overburden pressure, though surface tension allows for the maintenance of porosity structure at depth (see Fig. 6(a2)–(a4)). Eventually at large enough

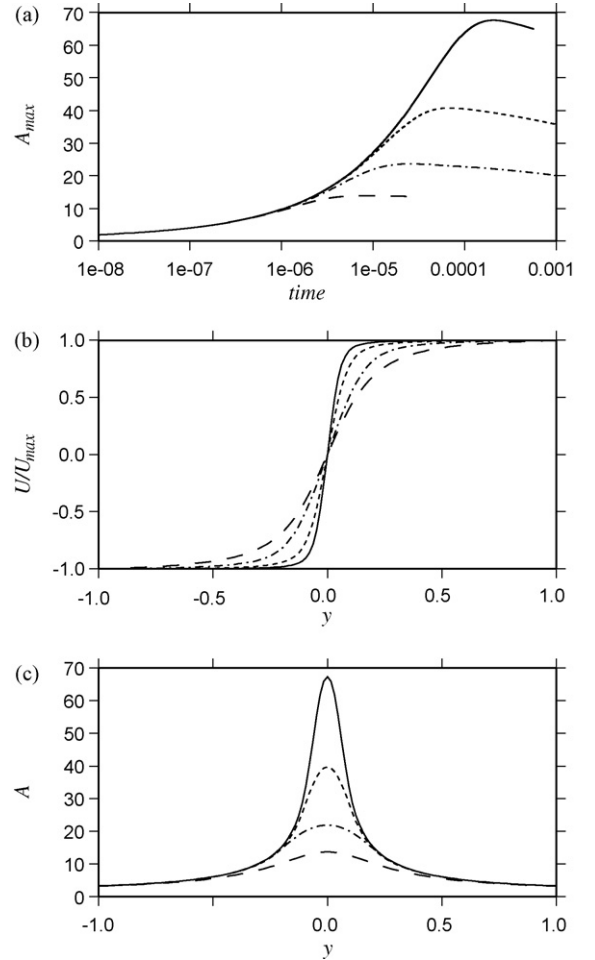


Fig. 5. (a) The maximum and minimum values of fitness versus time at constant damage fraction and shearing rate, but with different values of healing rate (\hat{k}_A). The value of $f_A = 10^{-1}$ and $U_{max} = 5 \times 10^4$, and the three different values of \hat{k}_A are 10^0 (solid), 10^1 (short dash), 10^2 (short dash-dot), and 10^3 (long dash). (b) The velocity into the shear zone, u , as a function of the horizontal coordinate y , normalized by U_{max} at a depth of $z = -0.5$. (c) The fitness across the shear zone at a depth of $z = -0.5$.

Bond numbers ($B \sim 1$) the porosity field separates totally from the matrix and the system becomes segregated. The addition of damage leads to a sharpening of the porosity profiles, though when the Bond number approaches one the effect of damage is less significant than the effect of gravity and the gross structure and location of porosity remain similar to cases without damage (Fig. 6). At small values of the Bond number, the porosity undergoes a more significant sharpening, while voids are suppressed at depth (Fig. 6(b2)). Cases with damage also evolve faster than cases without (Fig. 6(c1)–(c4)) even in the presence of non-zero B . The effect of gravity on void-generating damage therefore is to allow for similar types of localizing behavior as previously identified (Bercovici et al., 2001b; Bercovici and Ricard, 2003) at shallow depths and suppression of voids at depth. Though when the strength of overburden pressure is increased (by increasing B), gravity dominates over damage and leaves no remnant signal of localization from void-generating damage.

4.3. Void- and fitness-generating damage

We now examine the numerical results regarding how voids and fitness interact to allow for localization to vary as a function of both mechanism and depth.

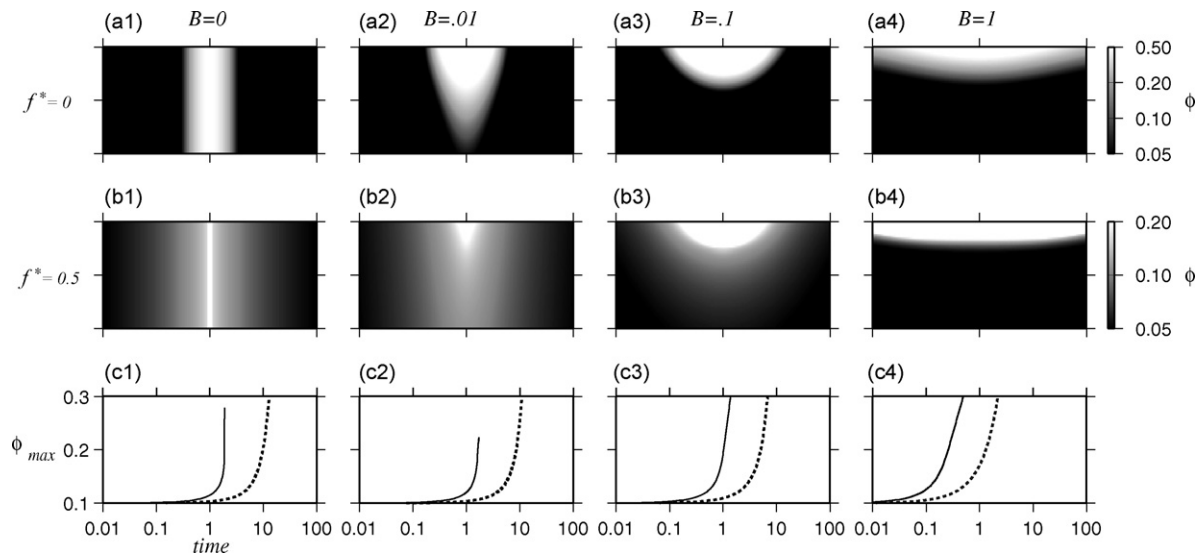


Fig. 6. The evolution of porosity with varying Bond number (B) and damage. The Bond number is constant for each column. (a1)–(a4) display the effect of gravity (through increasing B) in the absence of damage on the evolution of porosity. (b1)–(b4) display the effect of gravity and damage ($f^* = 0.5$, $\gamma = 10^4$, $U_{max} = 500$) on the evolution of porosity. (c1)–(c4) The time evolution of the maximum value of ϕ with varying B and damage ($f^* = 0$ (dashed) and $f^* = 0.5$ (solid)).

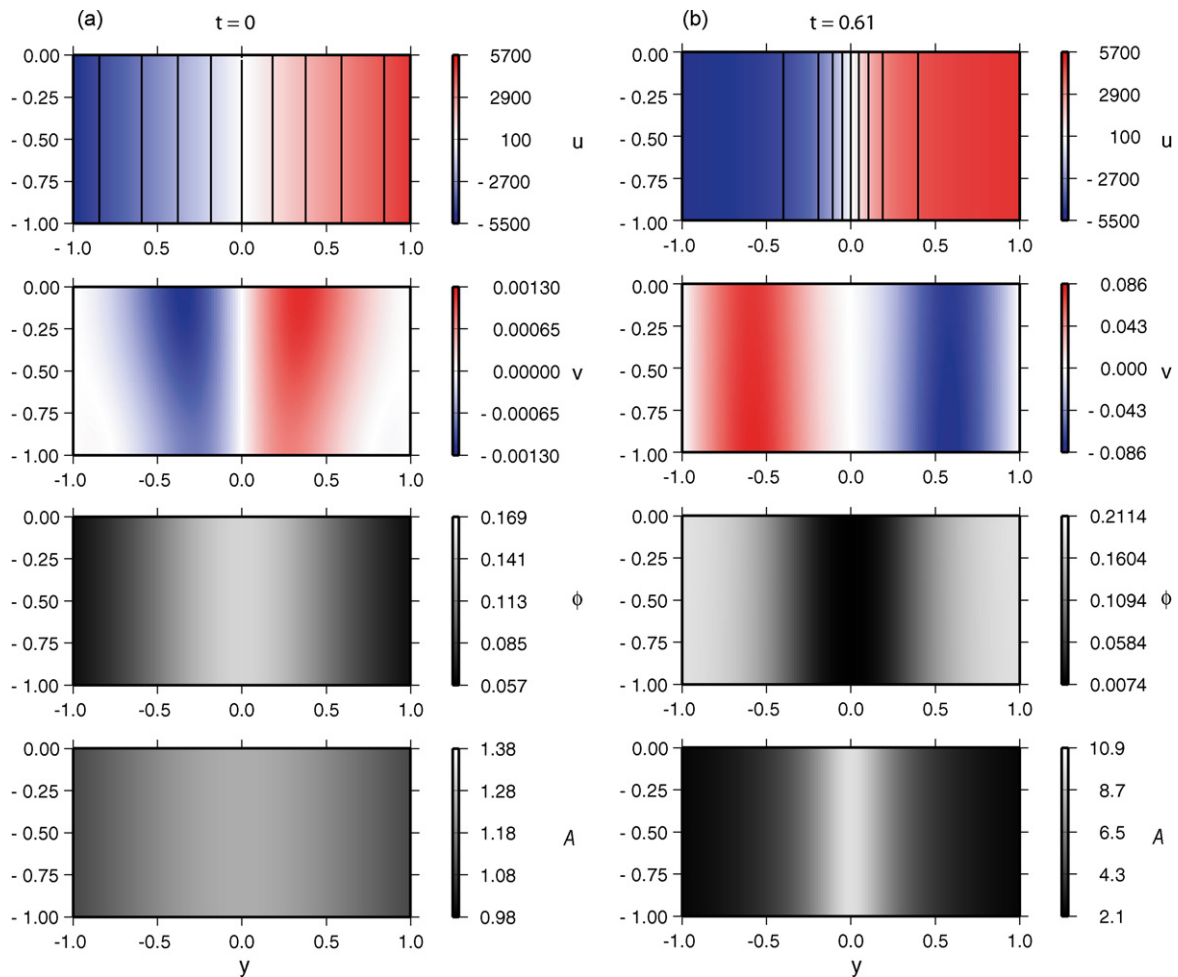


Fig. 7. The results at two different times for a case with both void- and fitness-generating damage. The relevant parameters for this run are $f_\phi = 0.5$, $f_A = 10^{-5}$, $\hat{k}_A = 10^{-3}$, $B = 10^{-2}$. The initial conditions are $\phi_o = 0.05$, $\phi_p = 0.1$, and $\delta_p = 0.5$ for porosity, and $A_o = 1.0$, $A_p = 0.25$, and $\delta_A = 1.0$ for fitness.

4.3.1. Time scale

Inspection of the results from pure void- and fineness-generating damage shows that the time evolution of the porosity and fineness fields can develop over vastly different scales (see Figs. 3 and 6). By choosing the void and fineness damage fraction to be of the same order ($f_A = f_\phi \approx .1$), the fineness field will evolve in time approximately four orders of magnitude faster. This suggests that the fineness field is far more efficient in generating damage and weakness than the porosity field. The reason for this temporal discrepancy is that the fineness field is not subject to the same mechanical constraints as the porosity field. The opening of voids via damage requires moving viscous matrix material, and this process must work against compaction and lithostatic pressure as well as obey mass conservation. On the contrary, the fineness field does not involve any volume expansion of the rock, hence it is far more efficient at converting deformational work into damage. In the following numerical simulations we choose the fineness and

void damage fraction to allow for the two fields to evolve on similar time scales.

4.3.2. Structure

Given the results of previous sections, one might expect that void and fineness-generating damage would superpose to allow greater localization at shallow depths, while deeper depths will give way to solely grain size inducing localization due to gravitational collapse of voids. However, in fact, the interaction of grain size reducing and void-generating damage results in the two modes of damage developing an anti-correlated structure (see ϕ and A in Fig. 7b). While the fineness field evolves in essentially the same manner as when $f_\phi = 0$, the porosity field evolves substantially differently than when $f_A = 0$. The end result is that grain size reduction leads to localized deformation and shear zone formation, while porosity is simultaneously forced out of the shear zone core and into the surrounding flanks (see Fig. 7).

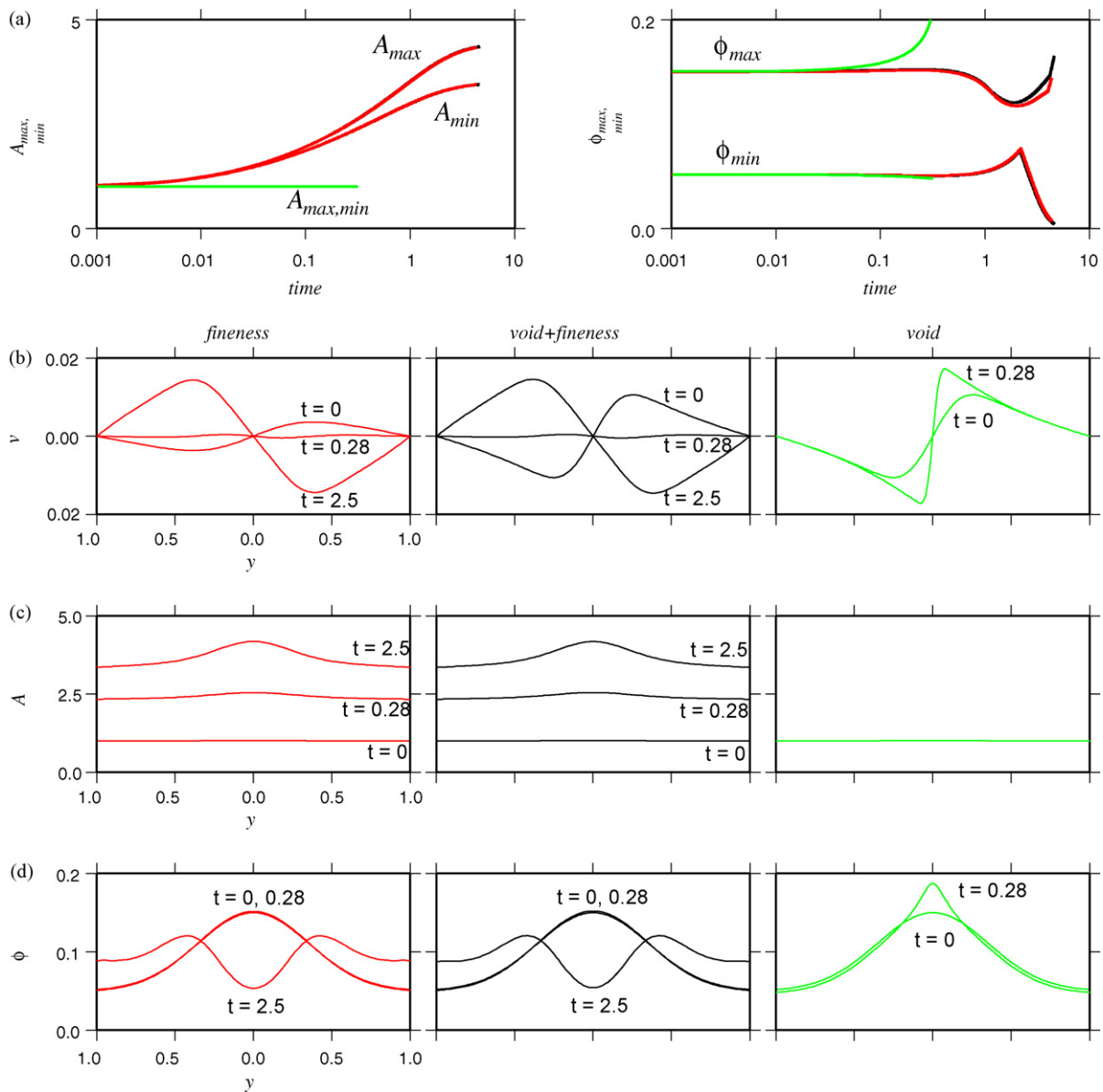


Fig. 8. A comparison of the evolution and behavior of fineness (red curves), void (green curves), and combined void- and fineness-generating damage (black curves) with the same initial conditions. (a) the time evolution of the maximum and minimum values of fineness and porosity. The results for ν (b), A (c), and ϕ (d) at a depth of $z = -0.5$ at three different times for cases with fineness-generating damage (left column), void-generating damage (right column), and both void- and fineness-generating damage (middle column). The relevant parameters for this run are $f^* = 0.5$, $\gamma = 10^6$, $f_A = 10^{-6}$, $k_A = 10^{-2}$, $B = 10^{-2}$. (For interpretation of the references to color in this figure legend, the reader is referred to the web version of the article.)

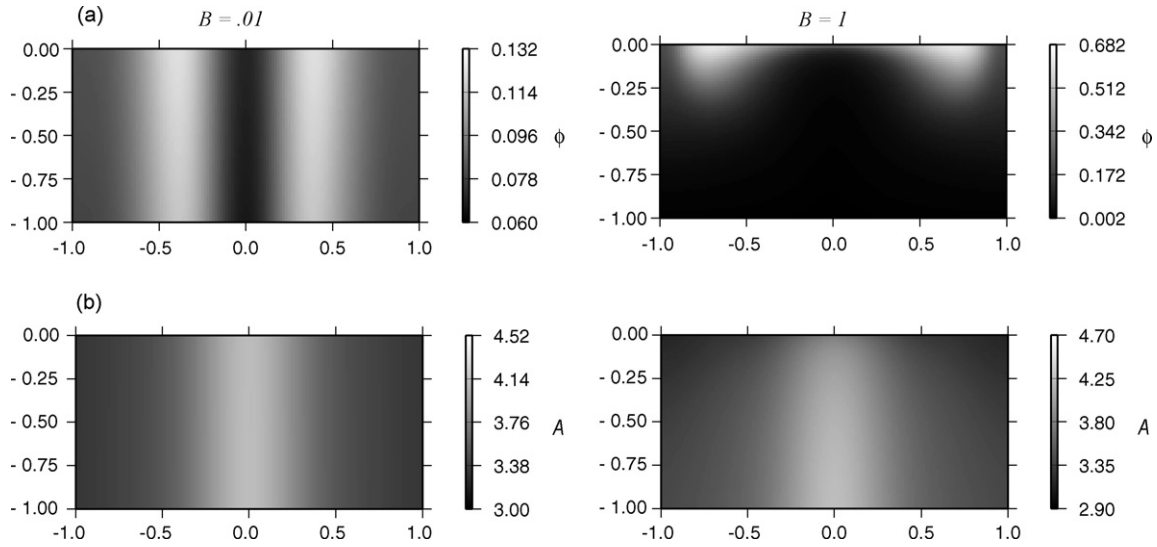


Fig. 9. A comparison of how varying the Bond number affects the porosity field with both void- and fineness-generating damage in effect. This figure displays the (a) porosity field and (b) the fineness field at $t = 2.3$ for the same set of initial conditions discussed in Fig. 8. The left column is for $B = 0.01$ and the right column is for $B = 1$. The relevant parameters for this run are $\phi_0 = 0.5$, $\gamma = 10^6$, $f_A = 10^{-6}$, $k_A = 10^{-2}$, and $U_{max} = 5 \times 10^3$.

The anti-correlated structure of the fineness and porosity fields can be understood by inspection of the forcing term on the left hand side of (17), $-\partial(A\lambda)/\partial y$, which is the driving force associated with surface tension. Evaluating the derivative with respect to y yields

$$\frac{\partial(A\lambda)}{\partial y} = -\lambda \frac{\partial A}{\partial y} - A(1 - \phi) \frac{d^2\eta}{d\phi^2} \frac{\partial \phi}{\partial y}, \quad (34)$$

where surface tension driven flow is associated with gradients in fineness (first term) and porosity (second term). The term $d^2\eta/d\phi^2$ is always less than zero (Ricard et al., 2001) while the other terms are greater than zero, hence the driving force arising from fineness gradients is opposite in sign to the force associated with porosity gradients. The physical process driving flow associated with porosity gradients can be understood as follows: The surface tension force (associated with porosity variation) is smaller in regions of higher porosity relative to lower porosity since this high porosity region has a smaller interfacial curvature. This surface tension difference causes a pressure gradient between regions of high and low porosity and is what drives the process of self-separation, thus subsequently driving the matrix away from regions of high porosity to areas of low porosity. The functional form for η assumed in this study guarantees that $d^2\eta/d\phi^2 < 0$, and is likely appropriate for the large dihedral angle voids assumed to constitute the secondary phase in this study. For low dihedral angle fluids, the functional form for η will likely differ and lead to a change in sign and hence a change in temporal evolution not predicted by this study (Hier-Majumder et al., 2006). This difference may be important for studying the evolution of shear zones with a fluid or melt secondary phase. Gradients in surface tension associated with gradients in fineness drive flow of the matrix from regions of low fineness to ones with high fineness since surface tension of reduced grain size material pulls harder than does that of coarser material (Bercovici and Ricard, 2005). Since the linear stability analysis predicts that the growth rate for both ϕ and A is in phase, the results from our numerical simulations imply that the anti-correlated nature of ϕ and A results from a finite amplitude effect. The non-linear surface tension term λA in (17) is linearized in the linear stability analysis, and therefore will not be able to predict this finite amplitude behavior. For many parameters explored in this study we find that the surface tension driving force associated with grain size variations overwhelms the effect due to porosity variations, therefore the resulting structure consists of a reduced grain size fault core surrounded by regions of higher porosity.

We examine the competition between gradients in fineness and porosity driven flow in greater detail at a small value of B ($= 10^{-2}$) (see Fig. 8). We start with an initial condition of $\phi_i = 0.05$, $\phi_p = 0.1$, and $\delta_p = 0.25$ in (33) for porosity, and $A_i = 1.0$, $A_p = 0.01$, and $\delta_A = 1.0$ in (32) for fineness. Gradients in porosity initially are greater in magnitude than gradients in fineness and drive matrix flow (v) away from $y = 0$ for void-generating damage, fineness-generating damage, and combined void- and fineness-generating damage ($t = 0$ in Fig. 8b). As gradients in fineness increase for fineness-generating and combined void- and fineness-generating damage ($t > 0$, Fig. 8c), the horizontal velocity v eventually becomes small for all y (see Fig. 8b at $t = 0.28$). If the fineness field does not vary from the initial conditions (due to $f_A = \hat{k}_A = 0$), then the horizontal velocity v and ϕ will evolve to form cusps and localization indicative of void-generating damage ($t = 0.28$ in Fig. 8b for void). Eventually the gradients in fineness become large enough to reverse matrix flow ($t = 2.5$ in Fig. 8b), and porosity is driven away from the center of the shear zone ($t = 2.5$ in Fig. 8d). The evolution of porosity with combined void- and fineness-generating damage therefore mirrors the evolution when there is only fineness-generating damage as the gradients in fineness grow. Unless variations in grain size are suppressed, the predictions from two-phase damage theory suggest that void-generation will predominantly form on the flanks of the shear zone due to grain size reduction in the central shear zone. By increasing the Bond number, the evolution of porosity deviates from the previous discussion. While porosity is still forced away from the center of the shear zone, increasing B results in lobes of porosity that decay with depth developing on the flanks of the shear zone (Fig. 9a). Therefore increasing B does not significantly alter the horizontal structure of porosity with combined void- and fineness-generating damage, and continues to suppress void-generation at depth.

5. Discussion and conclusion

We have explored the formation and structure of two-dimensional shear zones deforming under the influence of a rheology that is sensitive to both void-generation and grain size reduction. The goal has been to understand how these two forms of damage will facilitate localization at various depths in the lithosphere, and in this study we focus on how overburden pressure will

cause a change in the manifestations of damage. The salient results from this study include:

- (1) Grain size reducing damage is efficacious at producing localized structures, with the damage input (characterized by f_A and U_{max}) controlling the time scale for shear zone formation, and the ratio of damage input to healing (\hat{k}_A) controlling the final degree of localization attained.
- (2) For small values of Bond number $B = \rho g D / (\sigma A)$ ($< .1$), the suppression of void-generating damage at depth occurs while allowing for the localized behavior seen in 1D studies (Bercovici et al., 2001b; Bercovici and Ricard, 2003) at shallower depths. At larger values of B ($> .1$), the effect of gravity overwhelms damage and localization by void-generation fails to develop.
- (3) Combined void- and fineness-generating damage leads to the formation of anti-correlated porosity and fineness fields (see Fig. 7b), with the shear zone center characterized by reduced grain sizes and the flanks of the shear zone containing higher porosity regions.

The applicability of void- and grain size reducing damage to lithospheric dynamics and localization depends upon the reasonableness of the parameters specified (e.g. B , U_{max} , \hat{k}_A). We assume that the matrix is lithospheric silicate, therefore $\mu_o \approx 10^{25}$ Pa s (Beaumont, 1976), $\rho \approx 3 \times 10^3$ kg m $^{-3}$, and the depth of the shear zone, D , is approximately 50 km. The reference inverse grain size, A_o , is between 10^3 and 10^5 m $^{-1}$. While the value for the surface tension in silicates is commonly cited as 1 N m $^{-1}$ (Spry, 1983), the effective surface energy of fractures may be much higher, i.e., between 100 and 1000 N m $^{-1}$ (Atkinson, 1987; Atkinson and Meredith, 1987). Therefore the range of maximum Bond number, B , varies between 10 and 10^6 given the full lithospheric depth estimate used (decreasing the depth range obviously decreases the Bond number). This suggests that gravity will tend to dominate over void-generating damage in porosity evolution at mid- to deep lithospheric depths, and only at shallower depths (≥ 20 km) will void-generating damage be important. The range of values for the healing rate in pure olivine are on the order of 10^{-18} to 10^{-21} m 2 s $^{-1}$ (Karato, 1989), though the actual growth rate in a poly-mineralic assemblage will be smaller (Ohuchi and Nakamura, 2006). The non-dimensional healing rate, \hat{k}_A , therefore is of the range 10^3 – 10^8 , though it will likely be smaller due to the effect of secondary phases on grain growth mentioned above. Assuming tectonic velocities of 1 – 10 cm yr $^{-1}$, we estimate U_{max} between 10^2 and 10^8 , and f_A is between zero and one. The degree of localization goes approximately as $f_A U_{max}^2 / \hat{k}_A$, and the results from our simulations show that $f_A = 10^{-1}$, $U_{max} = 5 \times 10^4$ and $\hat{k}_A = 10^1$ (implying $f_A U_{max}^2 / \hat{k}_A \sim 10^5$) produces significant localization (Fig. 4). While the timescale given by $4\mu_o / (3\sigma A_o)$ implies lithospheric processes would be of the order of 100 Myr to 10 Byr, grain size reducing damage can allow a decrease in the localization time scale by either increasing f_A or U_{max} to facilitate shear zone formation in as little as 10 kyr. The parameter estimates for the lithosphere therefore suggest that grain size reducing damage can readily lead to significant shear localization on a relevant time scale consistent with plate boundary formation by considering the results from our study.

A common observation in fault zones is the development of grain size reduction in the fault core with lower porosity and permeability than is found in the surrounding protolith (Chester et al., 1993; Caine et al., 1996). The process of surface tension driven separation of grain size reduction and porosity structures found in our two-phase damage models may be applicable to understanding these observations from the brittle field. One may argue that the observations seen in fault zones reflect that smaller grains are able to more efficiently pack than the surrounding larger grain regions, but in a solid packing model ϕ does not depend on the grain size. The

predictions from our model therefore provide an explanation for the geological observations, and deserve further consideration in future studies.

The results from this study are intriguing, but further additions to our model need to be considered in future studies, the most obvious one being the consideration for how the depth-dependent variations in temperature will affect the formation of localization in the lithosphere, especially through its effect on grain size evolution. The extension of this study to two-dimensional domains is an important step, but further work needs to also consider different modes of deformation important in Earth (e.g. simple extension and compression). Given the results of this study and future directions discussed above, the application of void- and grain size reducing damage to lithospheric dynamics suggests a better understanding of how plate boundaries form and evolve is tractable.

Acknowledgments

Support was provided by the National Science Foundation (NSF, grant EAR-0537599). Reviews by Sash Hier-Majumder and an anonymous reviewer helped to clarify and improve the manuscript.

References

- Ashby, M., Sammis, C., 1990. The damage mechanics of brittle solids in compression. *Pure Appl. Geophys.* 133, 489–521.
- Atkinson, B., 1987. Introduction to fracture mechanics and its geophysical applications. In: Atkinson, B. (Ed.), *Fracture Mechanics of Rock*. Academic, San Diego, CA, pp. 1–26.
- Atkinson, B., Meredith, P., 1987. Experimental fracture mechanics data for rocks and minerals. In: Atkinson, B. (Ed.), *Fracture Mechanics of Rock*. Academic, San Diego, CA, pp. 427–525.
- Balachandar, S., Yuen, D., Reuteler, D., 1995. Localization of toroidal motion and shear heating in 3-D high Rayleigh number convection with temperature-dependent viscosity. *Geophys. Res. Lett.* 22, 477–480.
- Beaumont, C., 1976. The evolution of sedimentary basins on a viscoelastic lithosphere. *Geophys. J. R. Astron. Soc.* 55, 471–497.
- Bercovici, D., 1996. Plate generation in a simple model of lithosphere–mantle flow with dynamic self-lubrication. *Earth Planet. Sci. Lett.* 144, 41–51.
- Bercovici, D., 2003. The generation of plate tectonics from mantle convection. *Earth Planet. Sci. Lett.* 205, 107–121.
- Bercovici, D., Ricard, Y., 2003. Energetics of a two-phase model of lithospheric damage, shear localization and plate-boundary formation. *Geophys. J. Intl.* 152, 581–596.
- Bercovici, D., Ricard, Y., 2005. Tectonic plate generation and two-phase damage: void growth versus grain size reduction. *J. Geophys. Res.* 110, 1–18.
- Bercovici, D., Ricard, Y., Schubert, G., 2001a. A two-phase model of compaction and damage. 1. General theory. *J. Geophys. Res.* 106 (B5), 8887–8906.
- Bercovici, D., Ricard, Y., Schubert, G., 2001b. A two-phase model of compaction and damage. 3. Applications to shear localization and plate boundary formation. *J. Geophys. Res.* 106 (B5), 8925–8940.
- Braun, J., Chery, J., Poliakov, A., Mainprice, D., Vauchez, A., Tomassi, A., Daignieres, M., 1999. A simple parameterization of strain localization in the ductile regime due to grain size reduction: a case study for olivine. *J. Geophys. Res.* 104, 25167–25181.
- Caine, J., Evans, J., Forster, C., 1996. Fault zone architecture and permeability structure. *Geology* 24 (11), 1025–1028.
- Chester, F., Evans, J., Biegel, R., 1993. Internal structure and weakening mechanisms of the San Andreas fault. *J. Geophys. Res.* 90, 771–786.
- Hier-Majumder, S., Ricard, Y., Bercovici, D., 2006. Role of grain boundaries in magma migration and storage. *Earth Planet. Sci. Lett.* 248, 735–749.
- Jin, D., Karato, S., Obata, M., 1998. Mechanisms of shear localization in the continental lithosphere: inference from the deformation microstructures of peridotites from the Ivrea zone, northwestern Italy. *J. Struct. Geol.* 20, 195–209.
- Kameyama, M., Yuen, D., Fujimoto, H., 1997. The interaction of viscous heating with grain-size dependent rheology in the formation of localized slip zones. *Geophys. Res. Lett.* 24, 2523–2526.
- Karato, S., 1989. Grain growth kinetics in olivine aggregates. *Tectonophysics* 168, 255–273.
- Kohlstedt, D., Evans, B., Mackwell, S., 1995. Strength of the lithosphere: constraints imposed by laboratory experiments. *J. Geophys. Res.* 100, 17,587–17,602.
- Landuyt, W., Bercovici, D., Ricard, Y., 2008. Two-phase damage theory and plate generation in a 2D model of mantle convection. *Geophys. J. Intl.*, doi:10.1111/j.1365-246X.2008.03844.x.
- Lyakhovskiy, V., Ben-Zion, Y., Agnon, A., 1997. Distributed damage, faulting, and friction. *J. Geophys. Res.* 102, 27, 635–27, 649.
- McKenzie, D., 1984. The generation and compaction of partially molten rock. *J. Petrol.* 25, 713–765.

- Montesi, L., Hirth, G., 2003. Grain size evolution and the rheology of ductile shear zones: from laboratory experiments to postseismic creep. *Earth Planet. Sci. Lett.* 211, 97–110.
- Ohuchi, T., Nakamura, M., 2006. Grain growth in the forsterite-diopside system. *Phys. Earth. Planet. Int.* 160, 1–21.
- Paterson, M., 1978. *Experimental Rock Deformation: The Brittle Field*. Springer, Berlin.
- Poirier, J.-P., 1980. Shear localization and shear instability in materials in the ductile field. *J. Struct. Geol.* 2, 135–142.
- Regenauer-Lieb, K., 1998. Dilatant plasticity applied to Alpine collision: ductile void growth in the intraplate area beneath the Eifel volcanic field. *J. Geodyn.* 27, 1–21.
- Regenauer-Lieb, K., Yuen, D., 2003. Modeling shear zones in geological and planetary sciences: solid- and fluid- thermal–mechanical approaches. *Earth Sci. Rev.* 63, 295–349.
- Ricard, Y., Bercovici, D., 2003. Two-phase damage theory and crustal rock failure: the theoretical 'void' limit, and the prediction of experimental data. *Geophys. J. Int.* 155, 1057–1064.
- Ricard, Y., Bercovici, D., 2008. A continuum theory of grain size evolution and damage. *J. Geophys. Res.*, 2009, doi:10.1029/2007JB005491.
- Ricard, Y., Bercovici, D., Schubert, G., 2001. A two-phase model of compaction and damage. 2. Applications to compaction, deformation, and the role of interfacial surface tension. *J. Geophys. Res.* 106 (B5), 8907–8924.
- Spry, A., 1983. *Metamorphic Textures*. Pergamon, New York.
- Thatcher, W., England, P., 1998. Ductile shear zones beneath strike-slip faults—implications for the thermomechanics of the San Andreas fault zone. *J. Geophys. Res.* 103, 891–905.
- Yuen, D., Schubert, G., 1978. Shear heating instability in the Earth's upper mantle. *Tectonophysics* 50, 197–205.